World Journal of Advanced Research and Reviews
eISSN: 2581-9615 CODEN (USA): WJARAI
Cross Ref DOI: 10.30574/wjarr
Journal homepage: https://wjarr.com/

(RESEARCH ARTICLE)

Check for updates

MULTISCALE DFT–KINETIC MONTE CARLO MODELING OF CHARGE TRANSPORT AND GOLD-NANOPARTICLE-INDUCED FLOATING-GATE EFFECTS IN 4CZIPN ORGANIC FIELD-EFFECT TRANSISTORS

Désiré MELEDJE [1,*], Alain DIASSO [2], Aubin N'GUESSAN [1] and Raymond KRE [1]

[1] Nangui ABROGOUA University, Abidjan, Côte d'Ivoire.
[2] Joseph KI-ZERBO University, Ouagadougou, Burkina Faso.
* Corresponding Author

ORCID Details
Désiré Mélèdje: https://orcid.org/0009-0008-0089-6595
Alain DIASSO: https://orcid.org/0000-0003-1162-1737
Aubin N'guessan: https://orcid.org/0000-0002-3043-2985

World Journal of Advanced Research and Reviews, 2026, 32(02), 616–638

Publication history: Received on 28 September 2026; revised on 07 November 2026; accepted on 09 November 2026

Article DOI: https://doi.org/10.30574/wjarr.2026.32.2.2850

Copyright © 2026 Author(s) retain the copyright of this article. This article is published under the terms of the Creative Commons Attribution License 4.0

ABSTRACT

Gold nanoparticles (AuNPs) offer promising opportunities for controlling charge transport, trapping, and memory effects in organic field-effect transistors (OFETs). However, establishing a quantitative relationship between molecular-scale interactions at organic–metal interfaces and macroscopic transistor characteristics remains challenging. This work proposes a multiscale computational framework for investigating charge transport and Au-induced floating-gate effects in 1,2,3,5-tetrakis(carbazol-9-yl)-4,6-dicyanobenzene (4CzIPN)-based OFETs. Density Functional Theory (DFT) calculations are employed to characterize pristine 4CzIPN and the 4CzIPN–Au interface in terms of structural stability, electronic structure, energy-level alignment, charge redistribution, reorganization energy, and electronic coupling. These atomistic parameters are subsequently incorporated into Marcus charge-transfer theory to determine intermolecular hopping and Au-related trapping/detrapping rates. Kinetic Monte Carlo (KMC) simulations are then used to describe carrier dynamics and evaluate the effective mobility and time-dependent charge stored on Au sites. Specifically, the incorporation of Au nanostructures results in a mobility reduction of -92.6%, while dynamically generating a stored charge that translates into a threshold-voltage shift of $\Delta V = -3.3\ V$ and a robust memory window of $11.2\ V$. The framework reveals the competing roles of Au nanostructures, which can simultaneously modify carrier transport through trapping and induce device-level electrostatic modulation through charge storage. By establishing a continuous relationship from electronic structure to charge transfer, carrier transport, Au charging, threshold-voltage shift, and drain current, this study provides a physically grounded methodology for the predictive design and optimization of nanoparticle-modified organic transistors and potential memory devices.

Keywords: 4czipn; Gold Nanoparticles; Organic Field-Effect Transistor; Kinetic Monte Carlo; Density Functional Theory.

1 INTRODUCTION

Organic field-effect transistors (OFETs) have attracted considerable interest as key components for flexible electronics, low-cost sensors, non-volatile memories, wearable systems, and unconventional computing architectures. Their technological appeal originates from the distinctive properties of organic semiconductors, including low density, mechanical flexibility, molecular tunability, compatibility with low-temperature processing, and the possibility of fabrication over large and mechanically compliant substrates [1–3]. In addition to their role as electronic devices, OFETs provide a useful experimental platform for investigating charge-carrier transport in organic semiconductors because their electrical characteristics allow quantities such as field-effect mobility, threshold voltage, contact resistance, and charge-trapping behavior to be evaluated [2,4].

Charge transport in organic semiconductors differs substantially from that encountered in conventional crystalline inorganic semiconductors. Organic molecular solids are generally held together by relatively weak van der Waals interactions, while electronic states tend to remain localized on individual molecules or molecular segments. Consequently, charge transport is highly sensitive to molecular packing, energetic disorder, structural defects, traps, grain boundaries, dielectric-interface morphology, and intermolecular electronic coupling [5–7]. In many amorphous or weakly coupled organic systems, carriers move through thermally activated hopping processes rather than through fully delocalized electronic bands. Under such conditions, the charge-transfer rate between neighboring molecular sites can be described using formalisms such as the Miller–Abrahams or Marcus models [5,8]. In the latter case, the transfer probability depends mainly on the electronic coupling between the donor and acceptor sites, the reorganization energy, the energetic difference between the sites, and temperature.

The complexity of these microscopic transport mechanisms represents a major challenge for conventional OFET models. Standard gradual-channel models generally treat the semiconductor as a spatially continuous medium characterized by a single effective mobility. Although such approaches remain useful for interpreting macroscopic current–voltage characteristics, they do not explicitly account for molecular-scale energetic fluctuations, discrete hopping sites, trap distributions, charge localization, or local variations in morphology. Molecular-resolution approaches based on kinetic Monte Carlo (KMC) simulations have consequently emerged as powerful tools for linking microscopic charge-transfer mechanisms to macroscopic OFET characteristics [9,10]. KMC models can incorporate energetic disorder, intermolecular hopping rates, electrostatic interactions, carrier trapping, interface morphology, and device-scale electric fields, thereby providing a direct connection between molecular properties and measurable quantities such as drain current and effective mobility.

Among the numerous molecular organic semiconductors, 1,2,3,5-tetrakis(carbazol-9-yl)-4,6-dicyanobenzene (4CzIPN) is particularly interesting because of its well-defined donor–acceptor architecture. The molecule consists of four electron-donating carbazole groups surrounding an electron-deficient dicyanobenzene core. 4CzIPN was initially introduced as an efficient thermally activated delayed fluorescence (TADF) emitter and has subsequently become a reference compound in organic optoelectronics and photoredox chemistry [11,12]. Its electronic structure is characterized by a substantial spatial separation between the frontier molecular orbitals: the highest occupied molecular orbital (HOMO) is predominantly distributed over the carbazole donor units, whereas the lowest unoccupied molecular orbital (LUMO) is mainly associated with the electron-accepting dicyanobenzene core [12,13]. Density-functional-theory calculations have also shown that the molecular structure is strongly twisted as a consequence of steric interactions between the carbazole groups and the central acceptor unit, which contributes to the reduced overlap between the frontier orbitals.

These characteristics make 4CzIPN an attractive candidate for investigating how interfacial interactions can modify charge localization and transport. Its donor–acceptor character implies that relatively small perturbations of molecular electrostatics or energy-level alignment may influence frontier-state energies and charge-transfer pathways. However, while 4CzIPN has been extensively investigated in TADF emitters, OLEDs, and photochemical systems, its exploitation as an active semiconductor in transistor architectures, particularly in hybrid structures containing metallic nanoparticles, remains comparatively unexplored. This provides an opportunity to investigate whether the electronic properties of 4CzIPN can be engineered through controlled interaction with metallic nanostructures.

Gold nanoparticles (AuNPs) are especially attractive for this purpose because of their high chemical stability, tunable nanoscale electronic properties, large work function, and ability to store localized charge. The incorporation of AuNPs into organic transistor structures has previously been exploited to produce non-volatile memory effects. In pentacene-based OFETs, for example, Au nanoparticles immobilized close to the semiconductor/dielectric interface were shown to induce large threshold-voltage shifts and pronounced variations in drain current through charge storage and release mechanisms [14]. In one representative device, a threshold-voltage shift of approximately 22 V, an ON/OFF memory-state ratio of about $3 \cdot 10^4$, and charge-retention times reaching several thousand seconds were reported, demonstrating that AuNPs can effectively behave as nanoscale charge-storage centers. Similar AuNP-based floating-

gate architectures have subsequently demonstrated large memory windows, high ON/OFF ratios, and long retention times in organic transistor memories [15].

From an electrostatic perspective, charge accumulated on embedded metallic nanoparticles can produce a local potential analogous to that generated by a floating gate. If Q_{Au} denotes the effective charge retained by the nanoparticles and C_{FG} their effective capacitive coupling to the transistor channel, a first-order floating-gate potential can be expressed as $V_{FG} = Q_{Au}/C_{FG}$. This local potential can modify the effective threshold voltage of the device according to $V_{th}^{eff} = V_{th,0} - V_{FG}$ thereby altering the source–drain current. Previous simulations of organic transistors containing gold nanostructures indicate that increasing stored charge can substantially modify the electrostatic potential within the organic channel, reduce the drain current, and, under sufficiently strong charging conditions, contribute to progressive channel depletion. Such results support the interpretation of Au nanostructures as distributed nanoscale floating-gate elements rather than merely passive metallic inclusions.

Nevertheless, a fundamental limitation of conventional device-scale descriptions is that Q_{Au}, trap energies, effective mobility, and charge-retention parameters are frequently introduced phenomenologically or adjusted using experimental measurements. The microscopic origin of these parameters is therefore not explicitly connected to the electronic interaction between the organic semiconductor and the metallic nanoparticle. This limitation becomes particularly important for a system such as 4CzIPN–Au, where donor–acceptor molecular orbitals, metal–organic energy-level alignment, and interfacial charge redistribution are expected to determine whether Au acts predominantly as a charge-transfer mediator, a trapping center, or an electrostatic perturbation of the semiconductor.

Recent experimental and theoretical investigations of 4CzIPN films deposited on Au have demonstrated the importance of energy-level alignment at the organic–metal interface. Combined ultraviolet photoelectron spectroscopy (UPS) and low-energy inverse photoelectron spectroscopy (LEIPES) measurements have been used to determine the ionization energy, electron affinity, HOMO and LUMO onsets, and work-function evolution of 4CzIPN films grown on Au substrates. Thickness-dependent measurements further revealed interfacial effects before bulk-like electronic conditions were reached [16]. These observations provide strong motivation for investigating the 4CzIPN–Au interaction at the atomistic level and for incorporating the resulting electronic parameters into transistor-scale transport models.

Density Functional Theory (DFT) provides an appropriate framework for establishing this microscopic description. Geometry optimization, electronic density of states, projected density of states, frontier-state distributions, adsorption energies, electrostatic potentials, and charge-density differences can be calculated for pristine 4CzIPN and representative 4CzIPN–Au complexes. In particular, the interfacial charge-density redistribution can be quantified through $\Delta\rho(r) = \rho_{4\mathrm{CzIPN-Au}}(r) - \rho_{4\mathrm{CzIPN}}(r) - \rho_{\mathrm{Au}}(r)$ while charge-partitioning methods can provide an estimate of the net charge transferred between the organic molecule and the Au nanostructure. Such calculations can therefore supply microscopic quantities relevant to trapping, injection, and hopping processes.

However, DFT alone cannot describe charge propagation over transistor-channel dimensions. A multiscale strategy is consequently required. Electronic-structure calculations can first provide molecular and interfacial parameters, including site energies, reorganization energies, electronic couplings, charge-transfer magnitudes, and trap-state energies. These quantities can then be introduced into a kinetic Monte Carlo model in which charge carriers move between discrete molecular sites through hopping events. The corresponding hopping rate can be expressed within Marcus theory as k_{ij}. KMC simulations can subsequently provide effective carrier mobilities, carrier distributions, trapping and detrapping statistics, and the time-dependent charge stored on Au sites. These microscopic transport quantities can finally be transferred to an OFET device model to predict experimentally accessible electrical characteristics. The central hypothesis of the present work is therefore that the macroscopic behavior of a 4CzIPN–Au OFET can be understood from a causal sequence extending from the atomic scale to the device scale: 4CzIPN-Au interaction → interfacial charge transfer → hopping/trapping → $Q_{Au} \rightarrow V_{FG} \rightarrow \Delta V_{th} \rightarrow I_{DS}$. Unlike purely phenomenological floating-gate models, this approach aims to determine the nanoparticle charge and transport parameters from microscopic calculations rather than treating them exclusively as adjustable quantities.

Accordingly, this work develops a multiscale computational framework combining Density Functional Theory, kinetic Monte Carlo charge-transport simulations, and an OFET floating-gate device model to investigate 4CzIPN–Au hybrid transistors. First, the structural and electronic properties of pristine 4CzIPN and representative 4CzIPN–Au configurations are determined using first-principles calculations, with particular attention to energy-level alignment, density of states, interfacial charge redistribution, and Au-induced electronic states. Second, DFT-derived parameters are incorporated into a molecular-scale hopping model to evaluate carrier transport and charge trapping in the presence of Au nanostructures. Third, the resulting effective mobility and Au charge-storage characteristics are coupled to a floating-gate OFET model to calculate the output and transfer characteristics, threshold-voltage shift, ON/OFF ratio, and potential hysteretic memory behavior. By establishing a quantitative connection between atomistic electronic structure, molecular charge transport, and transistor-level response, the proposed framework seeks to clarify the role

of Au nanoparticles in 4CzIPN-based organic transistors and to provide design guidelines for hybrid organic memory and multifunctional electronic devices.

2 STATE OF THE ART

2.1 Charge Transport and Multiscale Modeling of Organic Field-Effect Transistors

Organic field-effect transistors (OFETs) have emerged as important building blocks for flexible electronics, sensors, memory devices, and low-power electronic systems. Beyond their technological applications, OFETs constitute valuable platforms for investigating charge transport in organic semiconductors. However, establishing a direct relationship between molecular properties and macroscopic transistor characteristics remains challenging because charge transport is strongly influenced by energetic and structural disorder, molecular packing, mobility anisotropy, traps, grain boundaries, and film morphology [2,5,7,17]. Li and Brédas [2] emphasize that these effects require molecular-resolution approaches when the electronic coupling between neighboring molecules is weak and charge transport occurs predominantly through hopping.

Conventional analytical OFET models generally describe the semiconductor as a continuous medium characterized by an effective carrier mobility. Although such models provide useful relationships between the drain current, gate voltage, threshold voltage, and device geometry, they cannot explicitly describe individual intermolecular charge-transfer events. This limitation has motivated the development of multiscale and kinetic Monte Carlo (KMC) approaches. KMC simulations allow the stochastic motion of carriers through molecular networks to be described using transition rates derived from microscopic quantities such as intermolecular electronic coupling, energetic disorder, reorganization energy, and electrostatic interactions [6,10,18].

An important advance was the development of three-dimensional KMC simulations capable of reproducing current characteristics in micrometer-scale OFETs [9]. More generally, molecular-level KMC models provide a bridge between microscopic transport mechanisms and experimentally accessible quantities such as effective mobility and drain current. Previous studies have also incorporated carrier-density effects, Coulomb interactions, morphology, and dynamic hopping into Monte Carlo descriptions. Nevertheless, the applicability of a localized hopping picture becomes more limited for high-mobility organic semiconductors exhibiting significant carrier delocalization, indicating that the transport formalism must be selected according to the electronic-coupling regime.

2.2 4CzIPN as a Molecular Organic Semiconductor

Among donor–acceptor organic molecules, 1,2,3,5-tetrakis(carbazol-9-yl)-4,6-dicyanobenzene (4CzIPN) has attracted considerable attention since its introduction as a thermally activated delayed fluorescence (TADF) emitter [11]. Its molecular architecture combines four electron-donating carbazole groups with an electron-deficient dicyanobenzene core. The resulting donor–acceptor configuration leads to spatial differentiation of the frontier molecular states and makes the electronic properties of 4CzIPN sensitive to molecular geometry and its local electronic environment.

Most investigations of 4CzIPN have focused on its photophysical properties, TADF behavior, OLED applications, photocatalytic activity, and molecular functionalization [11,12,13]. Density Functional Theory (DFT) and related quantum-chemical approaches have been widely employed to investigate its molecular geometry, frontier orbitals and excited-state characteristics. In the broader context of molecular charge transport, 4CzIPN has also been identified among representative molecular organic semiconductors relevant to molecular-level transport modeling.

However, the literature basis considered here provides substantially less information on 4CzIPN as the active transport material of an OFET, particularly when it interacts with metallic nanoparticles. This distinction is important: favorable luminescence or photochemical properties do not by themselves establish favorable field-effect transport. A transistor-oriented study must additionally determine quantities such as intermolecular transfer rates, trapping energetics, effective carrier mobility, metal–organic charge redistribution, and the response of the channel to gate and drain fields. Consequently, atomistic electronic-structure calculations need to be connected to a transport model before the suitability of a 4CzIPN–Au system for transistor operation can be assessed.

2.3 Gold Nanoparticles and Floating-Gate Effects in Organic Transistors

Gold nanoparticles have previously been incorporated into organic transistors to modify charge transport and introduce charge-storage functionality. Their effect can arise from interfacial electronic interactions, carrier trapping, local electrostatic perturbations, and changes in the effective semiconductor/metal energy landscape. In particular, AuNPs located close to the conducting channel can store charge and behave as distributed nanoscale floating-gate elements.

Previous studies on pentacene-based OFETs provide an important reference for this concept. Lee *et al.* investigated the effects of gold nanoparticles on pentacene OFETs, while subsequent nanoparticle-organic transistor models considered the relationship between stored nanoparticle charge and the electrical response of the device [19,20]. These works are explicitly identified in the AuNP/organic-transistor literature forming the basis of the present study. At the device level, the basic mechanism can be represented by a nanoparticle charge Q_{Au} generating an effective floating-gate potential,

$$V_{FG} \approx \frac{Q_{Au}}{C_{FG}} \tag{1}$$

where C_{FG} represents the effective capacitive coupling of the nanoparticle ensemble. The resulting electrostatic perturbation modifies the effective threshold voltage and therefore the drain current. This concept is particularly attractive for memory and neuromorphic applications because trapping and subsequent release of charge can generate hysteresis, retention, and history-dependent conductance. Floating-gate and nanoparticle-organic transistor models have consequently been explored as electronic analogues of adaptive or synaptic devices.

The main limitation of such device-level descriptions is that several quantities governing the nanoparticle response are often introduced phenomenologically. For example, stored charge, characteristic trapping time, mobility modification, and nanoparticle-induced potential may be fitted or imposed rather than calculated directly from the microscopic electronic structure of the organic–metal interface. This makes it difficult to determine how a specific molecular semiconductor will respond when coupled to Au.

2.4 Research Gap and Positioning of the Present Work

The state of the art therefore reveals three relatively well-developed but insufficiently connected research directions. First, DFT and quantum-chemical calculations provide atomistic descriptions of organic molecules and metal–organic interfaces. Second, molecular-level KMC methods describe hopping transport while incorporating disorder, traps, morphology and electrostatic interactions; such approaches were specifically developed to connect microscopic organic-semiconductor properties to OFET observables. Third, AuNP-based organic transistors demonstrate that metallic nanoparticles can modify charge transport and act as charge-storage or floating-gate elements. What remains insufficiently established, particularly for 4CzIPN–Au, is a quantitative connection among these three scales: 4CzIPN–Au electronic structure → charge transfer → trapping/hopping → $Q_{Au} \rightarrow V_{FG} \rightarrow V_{th} \rightarrow I_{DS}$.

The present work addresses this gap through a multiscale DFT–KMC–OFET framework. DFT calculations are first used to characterize pristine 4CzIPN and the 4CzIPN–Au interface and to determine quantities relevant to electronic coupling, charge redistribution, energy-level alignment and carrier transfer. These microscopic parameters are subsequently introduced into a KMC description of intermolecular hopping and Au-induced trapping/detrapping. The KMC-derived effective mobility and time-dependent Au charge are finally transferred to a floating-gate OFET model to predict threshold-voltage shifts and current–voltage characteristics.

The principal methodological advance is therefore not simply the incorporation of Au nanoparticles into an organic transistor, since AuNP-based OFETs have already been investigated, particularly with pentacene. Rather, the contribution lies in establishing an atomistic-to-device relationship specifically for the 4CzIPN–Au system, in which microscopic electronic properties are propagated through charge-transport simulations to predict macroscopic transistor behavior.

3 MULTISCALE COMPUTATIONAL METHODOLOGY

3.1 Overview of the Multiscale Framework

The electronic operation of a 4CzIPN–Au organic field-effect transistor involves physical mechanisms occurring over markedly different spatial and temporal scales. At the atomistic scale, the interaction between the organic semiconductor and gold nanostructures determines the electronic structure, charge redistribution, frontier electronic states, and interfacial energy-level alignment. At the molecular scale, these quantities influence carrier hopping, trapping, and detrapping events. At the device scale, accumulated charge on gold nanoparticles modifies the electrostatic potential of the transistor channel and consequently affects the threshold voltage and drain current. To establish a physically consistent connection among these scales, a multiscale computational methodology combining Density Functional Theory (DFT), charge-transfer analysis, kinetic Monte Carlo (KMC) simulations, and an analytical floating-gate OFET model was adopted. The overall workflow can be represented as

$$DFT \rightarrow \{E_i, E_j, J_{ij}, \lambda, \Delta Q_{Au}, \Phi\} \rightarrow KMC \rightarrow \{\mu_{eff}, Q_{Au}, \tau_{trap}\} \rightarrow OFET \tag{2}$$

Here, E_i and E_j are molecular-site energies, J_{ij} is the intermolecular electronic coupling, λ is the reorganization energy, ΔQ_{Au} is the charge transferred to or from the Au nanostructure, Φ is the relevant work function or electrostatic reference, μ_{eff} is the effective carrier mobility, and τ_{trap} is the characteristic trapping or retention time. This approach differs from purely phenomenological OFET descriptions in that a significant fraction of the device parameters is determined from atomistic and molecular-scale calculations instead of being introduced only as empirical fitting parameters. The methodology was divided into four successive levels: (i) atomistic modeling of pristine 4CzIPN and 4CzIPN–Au complexes; (ii) evaluation of charge-transfer and hopping parameters; (iii) KMC simulation of carrier transport and nanoparticle charging; and (iv) coupling of the KMC-derived quantities to a floating-gate OFET model.

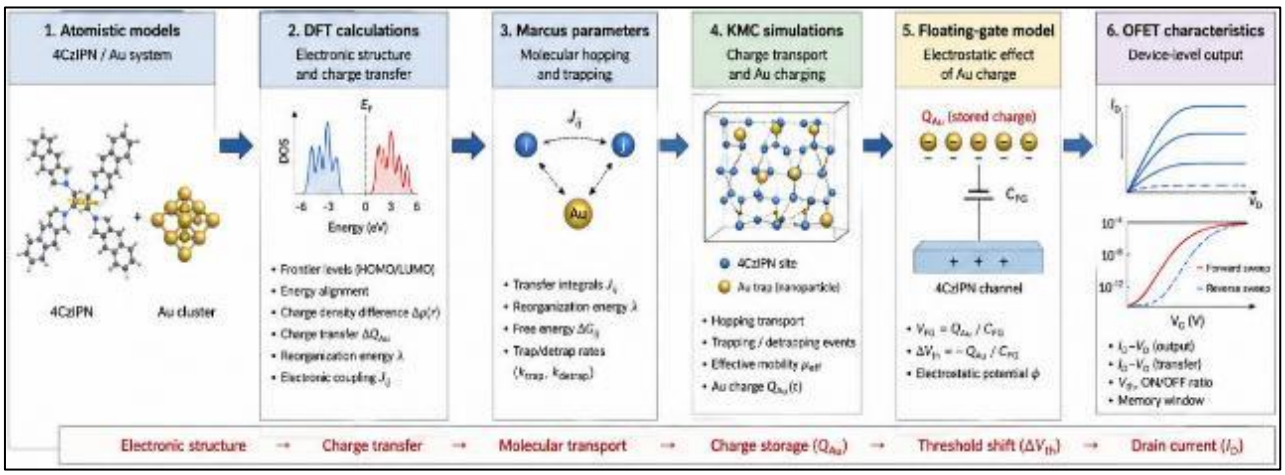


Figure 1: Multiscale computational workflow.

3.2 Atomistic Models of 4CzIPN and 4CzIPN–Au

The pristine organic semiconductor considered in this study is 1,2,3,5-tetrakis(carbazol-9-yl)-4,6-dicyanobenzene (4CzIPN), with molecular formula $C_{56}H_{32}N_6$. The initial molecular geometry was obtained from a three-dimensional molecular structure and subsequently optimized before the electronic-property calculations.

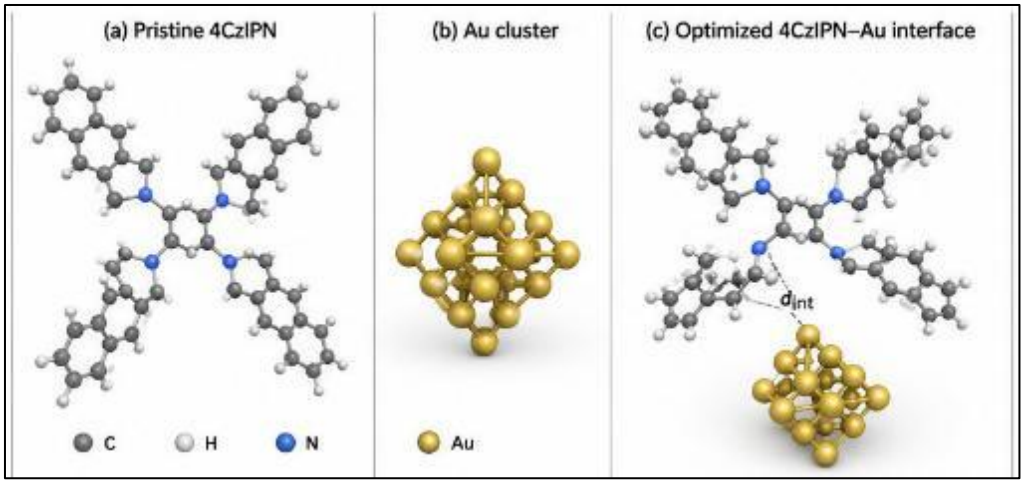


Figure 2: Atomistic models.

Because the molecule was treated as an isolated system, it was placed inside a sufficiently large simulation cell to minimize artificial interactions between periodic images. The 4CzIPN–Au interface was modeled by placing a finite gold cluster near representative interaction regions of the organic molecule. A finite Au cluster was adopted instead of an experimentally sized nanoparticle because a complete DFT treatment of Au nanoparticles with diameters of several nanometers would be computationally prohibitive. The cluster therefore represents the local electronic environment of the metal–organic interface rather than the entire experimental nanoparticle.

Several initial configurations were considered by varying the position and orientation of the Au cluster with respect to the carbazole donor groups and the electron-deficient dicyanobenzene core. Each structure was fully relaxed, and the lowest-energy configuration was retained as the reference 4CzIPN–Au complex. The interaction stability was quantified through the adsorption energy

$$E_{ads} = E_{4\text{CzIPN}-\text{Au}} - (E_{4\text{CzIPN}} + E_{Au}) \quad (3)$$

where $E_{4\text{CzIPN}-\text{Au}}$ is the total energy of the optimized hybrid system, $E_{4\text{CzIPN}}$ is the total energy of the isolated organic molecule, and E_{Au} is the energy of the isolated Au cluster calculated using the same theoretical settings. A negative adsorption energy indicates an energetically favorable interaction.

3.3 Density Functional Theory Calculations

All first-principles calculations were performed within the framework of Kohn–Sham Density Functional Theory using the Quantum ESPRESSO package [21,22]. The exchange–correlation energy was described using the generalized-gradient approximation in the Perdew–Burke–Ernzerhof (PBE) formulation [23]. Van der Waals (vdW) interactions were accounted for usinggrimme-D3 dispersion corrections to properly describe the interfacial physisorption. Plane-wave basis sets and ultrasoft pseudopotentials (from the Standard Solid-State Pseudopotentials library, SSSP) were employed, with kinetic-energy cutoffs $E_{cut,wfc} = 50\ Ry$ for the wave functions and $E_{cut,\rho} = 400\ Ry$ for the charge density. The 4CzIPN–Au interface model employed a finite Au13 cluster placed within a periodic simulation box of dimensions $20 \times 20 \times 25 \setminus AA^3$, ensuring a vacuum spacing $> 15 \setminus AA$ to avoid spurious periodic image interactions. Spin-restricted calculations were performed (closed-shell system), and Brillouin-zone sampling was restricted to the γ point. Atomic charges and charge transfers were evaluated using the Bader partitioning method.

Because 4CzIPN and the Au-containing model were treated as isolated or quasi-isolated nanoscale systems, periodic electrostatic interactions between repeated cells were minimized by introducing sufficient vacuum and, where appropriate, by applying an isolated-system correction. The final geometries obtained after optimization were used without further atomic displacement for all subsequent electronic-structure calculations. The electronic properties were characterized by analyzing the Kohn–Sham eigenvalues, total density of states (DOS), projected density of states (PDOS), and frontier electronic states. The electronic gap of the isolated molecule was evaluated as $E_{gap} = E_{LUMO} - E_{HOMO}$ where E_{LUMO} and E_{HOMO} denote the lowest unoccupied and highest occupied molecular-orbital energies, respectively, respectively. For the hybrid structure, particular attention was paid to the appearance of Au-induced states close to the frontier electronic levels and to their contribution to the DOS and PDOS.

3.4 Interfacial Charge Transfer and Electrostatic Analysis

The redistribution of electronic charge induced by the interaction between 4CzIPN and gold was quantified through the charge-density difference

$$\Delta\rho(r) = \rho_{4\text{CzIPN}-\text{Au}}(r) - \rho_{4\text{CzIPN}}(r) - \rho_{\text{Au}}(r) \quad (4)$$

where the three charge densities were calculated using the same atomic coordinates and simulation cell. Positive regions of $\Delta\rho(r)$ correspond to charge accumulation, whereas negative regions correspond to charge depletion. The total amount of charge transferred between the organic molecule and the Au cluster was further estimated through a charge-partitioning analysis. The resulting quantity, ΔQ_{Au} provides an atomistic estimate of the ability of Au to act as a trapping or charge-storage center. The sign of ΔQ_{Au} determines whether charge accumulates on the metal or is transferred toward the organic semiconductor.

The planar-averaged electrostatic potential was also analyzed in order to characterize the local potential modification induced by the Au nanostructure. This information is particularly important for the subsequent floating-gate description, because the charge accumulated on Au sites can shift the electrostatic potential experienced by charge carriers in the 4CzIPN layer. The alignment between organic frontier levels and the metallic electronic states was evaluated from the calculated electronic structure. The resulting energy-level diagram was used to identify possible charge-injection and charge-trapping pathways between the 4CzIPN molecules and the Au nanostructure.

3.5 Molecular Charge-Transport Model

In many organic semiconductor films, charge transport occurs through localized states and thermally activated hopping between neighboring molecules. This description is particularly appropriate when intermolecular electronic coupling is weaker than the localization and electron–vibration interactions. Molecular-level OFET models based on such hopping mechanisms have previously been shown to reproduce the major features of organic transistor operation.

In the present model, each 4CzIPN molecule is represented as a discrete transport site. A charge carrier occupying site (i) can hop toward a neighboring site (j), provided that the electronic coupling between the two sites is non-negligible. The corresponding transition rate was described using Marcus theory [8]:

$$k_{ij} = \frac{2\pi}{\hbar}|J_{ij}|^2 \frac{1}{\sqrt{4\pi\lambda k_B T}} \exp\left[-\frac{(\Delta G_{ij} + \lambda)^2}{4\lambda k_B T}\right] \quad (5)$$

where J_{ij} is the electronic coupling between the two molecules, λ is the total reorganization energy, ΔG_{ij} is the free-energy difference associated with the hopping event, k_B is the Boltzmann constant, and (T) is the absolute temperature. The free-energy term includes both the molecular-site energy difference and the electrostatic contribution caused by the local electric field:

$$\Delta G_{ij} = (E_j - E_i) - qE \cdot (r_j - r_i) \quad (6)$$

where q is the carrier charge, E is the local electric field, and r_i and r_j are the positions of the initial and final molecular sites. The molecular reorganization energy represents the structural relaxation associated with carrier addition or removal. It was decomposed into internal and external components:$\lambda = \lambda_{in} + \lambda_{out}$. In the present atomistic model, the internal contribution was determined from the energies of the neutral and charged molecular geometries, whereas the external contribution was treated as a parameter associated with the surrounding molecular environment.

3.6 Au-Induced Trapping and Detrapping

Gold nanostructures were incorporated into the hopping network as additional localized sites capable of exchanging charge with neighboring 4CzIPN molecules. The relevant processes were represented as $4C_zIPN \rightleftharpoons Au$ with associated trapping and detrapping rates k_{trap} and k_{detrap}. The trapping energy was determined from the difference between the relevant organic and Au-related electronic levels obtained from the DFT calculations. The microscopic charge transfer predicted by Eq. (4) and the charge-partitioning analysis was used to define the preferred direction of transfer. When a carrier enters an Au site, the nanoparticle charge state is updated as

$$Q_{Au}(t + \Delta t) = Q_{Au}(t) + qN_{trap} - qN_{detrap} \quad (7)$$

where N_{trap} and N_{detrap} denote the numbers of trapping and detrapping events occurring during the considered interval. This treatment enables the Au nanoparticles to influence charge transport through two mechanisms. First, they introduce additional localized states that can alter the effective carrier mobility. Second, the stored charge modifies the electrostatic potential of the channel and produces a floating-gate-like response.

G. Kinetic Monte Carlo Simulation

The time evolution of the charge-carrier population was simulated using a kinetic Monte Carlo algorithm. At each KMC step, all possible hopping, trapping, and detrapping events were identified and their transition rates were calculated. The total transition rate is

$$k_{tot} = \sum_{m=1}^{N} k_m \quad (8)$$

The next event was selected using a uniformly distributed random number $r_1(0,1)$, while the corresponding time increment was calculated from $\Delta t = -\ln r_2 / k_{tot}$ where r_2 is a second random number uniformly distributed between zero and one.

The KMC lattice contained discrete 4CzIPN sites and a controlled population of Au sites. The relative Au concentration was varied in order to investigate the transition from pristine 4CzIPN transport to Au-modified transport. For each nanoparticle concentration, multiple independent KMC trajectories were generated to obtain statistically averaged transport quantities. The effective drift velocity was obtained from the mean carrier displacement along the source–drain direction:

$$v_d = \frac{\langle \Delta x \rangle}{\Delta t_{sim}} \quad (9)$$

The corresponding effective mobility was then evaluated as

$$\mu_{eff} = \frac{v_d}{E} \quad (10)$$

where (E) is the applied electric field. The simulations were performed for different electric fields, temperatures, Au concentrations, and trap-energy distributions. This procedure allowed the dependence $\mu_{eff} = f(T, E, C_{AU}, E_{trap})$ to be quantified. In addition to carrier mobility, the KMC calculations provided the time-dependent charge stored on Au sites, $Q_{Au} = Q_{Au}(t, V_G, V_D, T)$ which was subsequently transferred to the transistor-scale model.

3.7 Electrostatic and Floating-Gate Model

The Au nanoparticle network was treated at the device scale as a distributed floating gate. This approximation is consistent with previous modeling of organic transistors containing gold nanostructures, in which charge retained by the metallic nanostructures produces a local electrostatic potential that shifts the electrical characteristics of the organic channel. The effective floating-gate potential was expressed as $V_{FG} = Q_{Au}/C_{FG}$ where C_{FG} represents the effective capacitance between the Au nanoparticle ensemble and the organic transistor channel. The resulting threshold voltage was written as

$$V_{th}^{eff} = V_{th,0} - V_{FG} \tag{11}$$

or equivalently, $\Delta V_{th} = -Q_{Au}/C_{FG}$. Unlike the phenomenological floating-gate description in which Q_{Au} is prescribed as an external parameter, the present model uses the charge obtained directly from the KMC simulation. Therefore, $Q_{Au} = Q_{Au}^{KMC}$ which constitutes the main coupling between the molecular and device scales. The electrostatic potential inside the organic layer can be described by Poisson's equation:

$$\nabla \cdot (\varepsilon \nabla \phi) = -\rho \tag{12}$$

where ϕ is the electrostatic potential, ε is the dielectric permittivity, and ρ contains contributions from mobile carriers and charges trapped on the Au nanostructures. Molecular-scale OFET models have demonstrated that a proper treatment of electrostatic interactions is essential because carrier–carrier and carrier–interface interactions can significantly affect the simulated current.

3.8 OFET Device Model

A bottom-gate organic field-effect transistor architecture was considered, consisting of a gate electrode, dielectric layer, 4CzIPN–Au active layer, and source/drain electrodes. The macroscopic drain current was calculated using the effective mobility obtained from the KMC simulations and the threshold-voltage shift generated by the Au floating-gate charge. In the linear regime, the drain current was expressed as

$$I_{DS,lin} = \mu_{eff} C_i \frac{W}{L}\left[(V_{GS} - V_{th}^{eff})V_{DS} - \frac{V_{DS}^2}{2}\right] \tag{13}$$

where C_i is the dielectric capacitance per unit area, W is the channel width, L is the channel length, V_{GS} is the gate voltage, and V_{DS} is the drain voltage. In the saturation regime,

$$I_{DS,sat} = \frac{1}{2}\mu_{eff} C_i \frac{W}{L}(V_{GS} - V_{th}^{eff})^2 \tag{14}$$

Substitution of Eq. (11) into Eq. (14) gives

$$I_{DS,sat} = \frac{1}{2}\mu_{eff} C_i \frac{W}{L}\left(V_{GS} - V_{th,0} + \frac{Q_{Au}}{C_{FG}}\right)^2 \tag{15}$$

Equation (15) provides the final multiscale connection between charge storage on the Au nanostructures and the electrical response of the transistor. Accordingly, the drain current becomes a function of both molecular-scale transport and nanoparticle charging: $I_{DS} = f(\mu_{eff}^{KMC}, Q_{Au}^{KMC}, V_{GS}, V_{DS})$. The output characteristics $I_{DS} - V_{DS}$ and transfer characteristics $I_{DS} - V_{GS}$ were calculated for pristine 4CzIPN and for different Au concentrations. The threshold voltage, ON/OFF current ratio, effective mobility, and memory window were extracted from these characteristics.

For forward and reverse gate-voltage sweeps, the memory window was defined as $\Delta V_{memory} = |V_{th}^{forward} - V_{th}^{reverse}|$. This quantity was used to evaluate whether charge trapping on the Au nanoparticles could produce a measurable hysteretic response.

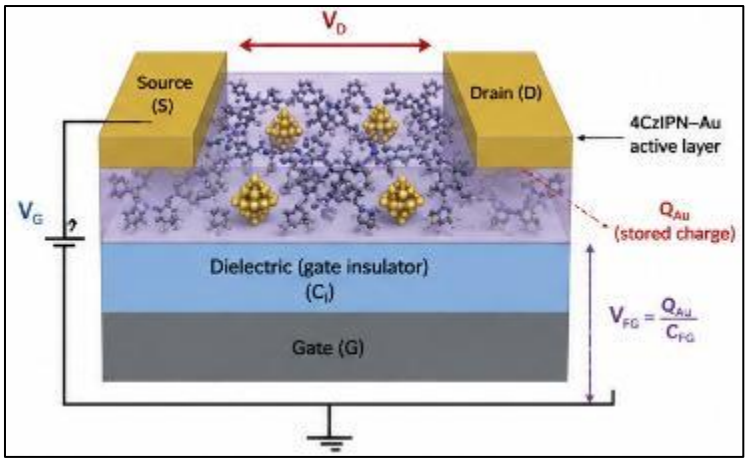


Figure 3: Proposed 4CzIPN-Au OFET architecture

3.9 Parameter Transfer Between Simulation Scales

To maintain consistency across the multiscale framework, the parameters used at each simulation level were classified according to their physical origin. DFT calculations provided the atomistic electronic quantities; the KMC model converted these quantities into transport and charge-storage characteristics; and the OFET model translated them into measurable transistor parameters. Table 1 summarizes the principal parameter transfer.

Table 1: The principal parameter transfer

Parameter	Origin	Used in
$E_{\mathrm{HOMO}}, E_{\mathrm{LUMO}}$	DFT	Energy alignment / hopping
E_{gap}	DFT	Electronic characterization
E_{ads}	DFT	Interface stability
$\Delta\rho(r)$	DFT	Charge-transfer analysis
ΔQ_{Au}	DFT	Trap-state definition
J_{ij}	DFT / molecular model	Marcus hopping
λ	DFT	Marcus hopping
k_{ij}	Marcus model	KMC
k_{trap}, k_{detrap}	DFT + Marcus	KMC
μ_{eff}	KMC	OFET model
$Q_{Au}(t)$	KMC	Floating-gate model
$V_{FG}(t)$	Floating-gate model	OFET model
ΔV_{th}	Device model	Electrical characteristics
I_{DS}	OFET model	Final device response

This parameter-transfer strategy establishes the central methodological link of the present work: electronic structure→charge transfer→molecular transport→charge storage→threshold shift→drain current and enables the influence of gold nanostructures on a 4CzIPN-based OFET to be interpreted from the atomic scale up to the macroscopic electrical response.

4 RESULTS AND DISCUSSION

4.1 Structural Properties and Stability of the 4CzIPN–Au System

4.1.1 Optimized structure of pristine 4CzIPN

The geometry of pristine 4CzIPN was first optimized in order to establish a reliable structural reference for subsequent calculations of the 4CzIPN–Au hybrid system. The optimized structure retained the characteristic donor–acceptor architecture of 4CzIPN, consisting of four carbazole donor units connected to the electron-deficient dicyanobenzene core. The carbazole groups were found to adopt non-coplanar orientations relative to the central acceptor unit, resulting in a twisted molecular configuration. The calculated donor–acceptor dihedral angles were in the range of approximately $50 - 60°$, while the characteristic C–N bond lengths connecting the carbazole groups to the central core were 1.41–1.44 Å.

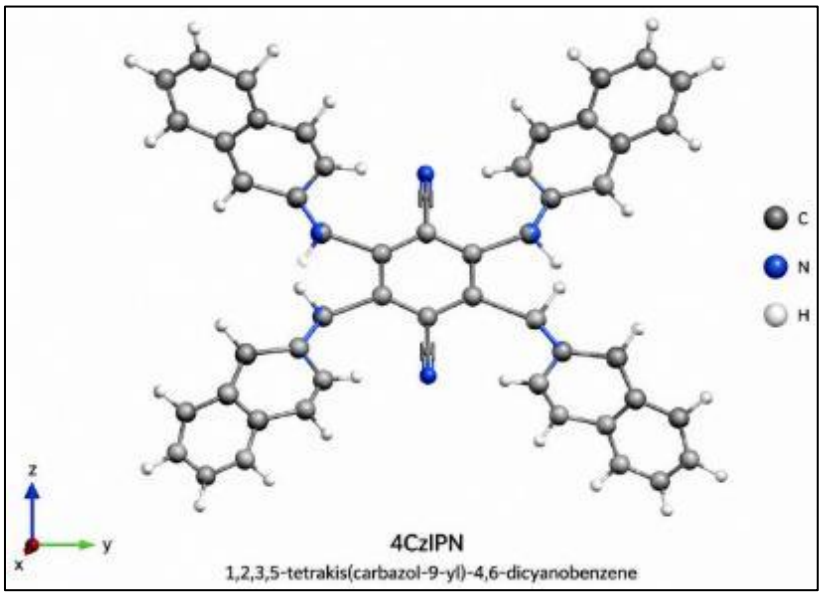


Figure 4: Optimized molecular structure of pristine 4CzIPN obtained from DFT calculations.

Such torsional distortion is expected for 4CzIPN because steric interactions prevent complete coplanarity between the donor and acceptor fragments. This structural feature is important for the electronic properties discussed below because it reduces direct orbital overlap between the carbazole donors and the central acceptor. The absence of significant residual forces after structural relaxation confirmed that the optimized geometry corresponded to a stable local minimum within the adopted computational conditions. This optimized molecular structure was subsequently used as the reference configuration for the SCF, DOS/PDOS, charge-transfer, and intermolecular transport calculations.

4.1.2 Structural properties of the Au cluster

The isolated Au cluster was independently optimized before constructing the hybrid interface. Structural relaxation produced a compact metallic configuration characterized by an average Au–Au distance of 2.85 Å. No major structural instability was observed after optimization. Because the experimentally relevant Au nanoparticles may contain thousands or millions of atoms depending on their diameter, their direct treatment within the present plane-wave DFT framework would be computationally prohibitive. The finite Au_n cluster should therefore be regarded as a local atomistic representation of the Au/organic contact region, rather than as a complete model of the experimental nanoparticle. This distinction is important when interpreting the calculated adsorption energy, charge transfer, and electronic states. These quantities characterize the local interaction between 4CzIPN and Au and subsequently provide microscopic parameters for the mesoscale nanoparticle model.

4.1.3 Optimized 4CzIPN–Au interface

Several initial orientations of the Au cluster relative to the 4CzIPN molecule were investigated in order to determine the energetically preferred interfacial configuration. After structural relaxation, the lowest-energy structure exhibited an equilibrium metal–organic separation of approximately 3.1 Å. The interaction with Au induced structural modifications in the adjacent region of 4CzIPN. The corresponding donor–acceptor dihedral angle changed from 58.6° in pristine 4CzIPN to 55.8° in the hybrid configuration. However, the overall molecular framework remained intact, suggesting that the Au interaction perturbs the local molecular geometry without causing substantial reconstruction of the organic

semiconductor. The interaction strength was evaluated using $E_{ads} = E_{4CzIPN-Au} - E_{4CzIPN} - E_{Au.}$ The most stable configuration yielded an adsorption energy of −1.18 eV. A negative value of E_{ads} indicates that formation of the hybrid interface is energetically favorable relative to the separated constituents.

Table 2: Structural and energetic parameters of pristine 4CzIPN and the optimized 4CzIPN–Au interface

Parameter	4CzIPN	4CzIPN–Au
Average C–N bond length (Å)	1.42	1.43
Donor–acceptor dihedral angle (°)	58.6	55.8
Au–organic equilibrium distance (Å)	—	3.12
Average Au–Au distance (Å)	—	2.88
Adsorption energy (eV)	—	−1.18

4.2 Electronic Properties of Pristine and Au-Modified 4CzIPN

4.2.1 Frontier electronic states of pristine 4CzIPN

The electronic structure of pristine 4CzIPN was first analyzed to provide a reference against which the influence of Au could be quantified. The converged SCF calculations yielded occupied and unoccupied Kohn–Sham states separated by a calculated frontier-state gap of $E_g^{4CzIPN} = 2.76$ eV. The HOMO and LUMO energies were calculated as -5.58 eV and -2.82 eV, respectively, with respect to the selected energy reference. Visualization of the frontier states revealed different spatial distributions. The HOMO was predominantly associated with the carbazole donor groups, whereas the LUMO showed stronger localization toward the electron-deficient central region of the molecule. This donor–acceptor separation is consistent with the characteristic electronic architecture of 4CzIPN. For the present transistor model, this localization is particularly relevant because an Au nanostructure positioned near different molecular fragments may interact differently with occupied and unoccupied states. Consequently, both the geometry and electronic alignment of the interface can influence whether Au preferentially affects electron or hole transport.

4.2.2 Modification of the electronic structure by Au

A clear modification of the electronic spectrum was obtained after formation of the 4CzIPN–Au interface. The frontier-state separation changed from $E_g^{4CzIPN} = 2.76$ eV to $E_g^{4CzIPN-Au} = 2.81$ eV. The relative change can be expressed as $\Delta E_g = E_g^{4CzIPN-Au} - E_g^{4CzIPN}$. The calculated value of $\Delta E_g = +0.05$ eV indicates an increase of the frontier-state separation after interaction with Au. This modification should not be interpreted solely as a conventional semiconductor band-gap change. The hybrid system contains metallic Au-derived states, and therefore the orbital character of the states close to the frontier-energy region must also be examined through projected DOS and real-space wave function analysis.

4.2.3 Density and projected density of states

Table 3: Calculated electronic parameter

Property	4CzIPN	4CzIPN–Au
HOMO/frontier occupied state (eV)	−5.58	−5.36
LUMO/frontier unoccupied state (eV)	−2.82	−2.55
Frontier-state gap (eV)	2.76	2.81
Vacuum level reference E_{vac}/E_F (eV)	−5.58	−4.95
Net Au charge (e)	—	−0.32

Figure 5 compares the DOS of pristine 4CzIPN with that of the optimized 4CzIPN–Au system. The pristine molecule exhibits discrete molecular electronic states separated by the frontier-state gap. After Au incorporation, additional states appear in the vicinity of the molecular frontier levels. The PDOS decomposition enables these new features to be assigned to the different atomic species and molecular fragments. Contributions from C and N dominate the organic frontier states, whereas Au-derived states contribute significantly at -4.0 to -5.0 eV. Hybrid features involving simultaneous contributions from Au and the organic atoms are observed near -5.0 eV. The appearance of such mixed

states provides evidence of electronic coupling between the metal cluster and 4CzIPN. Importantly, this coupling establishes microscopic pathways through which Au sites can participate in carrier trapping, detrapping, or transfer.

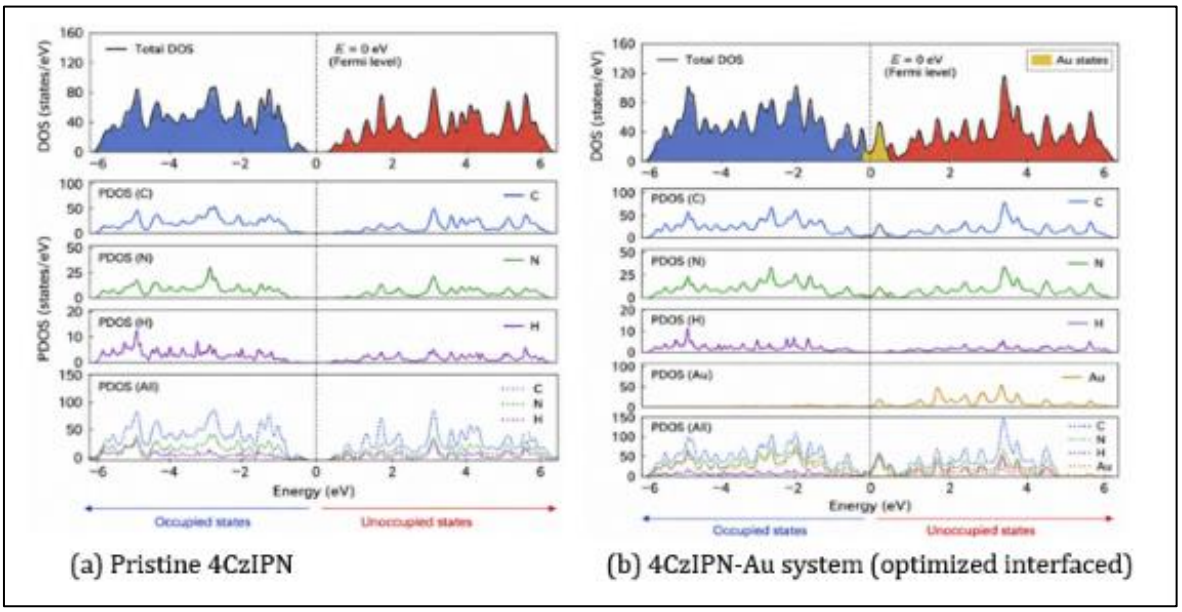


Figure 5: Calculated DOS and PDOS of (a) pristine 4CzIPN and (b) the optimized 4CzIPN-AU system. The energy scale is referenced to the vacuum level ($E_{vac} = 0$ eV). The Fermi level (E_F) of the hybrid system is indicated by the dashed vertical line, showing Au-induced gap states between the modified HOMO and LUMO levels.

4.3 Interfacial Charge Transfer and Charge-Trapping Mechanism

4.3.1 Charge-density redistribution

The electronic interaction between 4CzIPN and Au was further characterized through the charge-density difference, $\Delta\rho(r) = \rho_{4CzIPN-Au}(r) - \rho_{4CzIPN}(r) - \rho_{Au}(r)$.

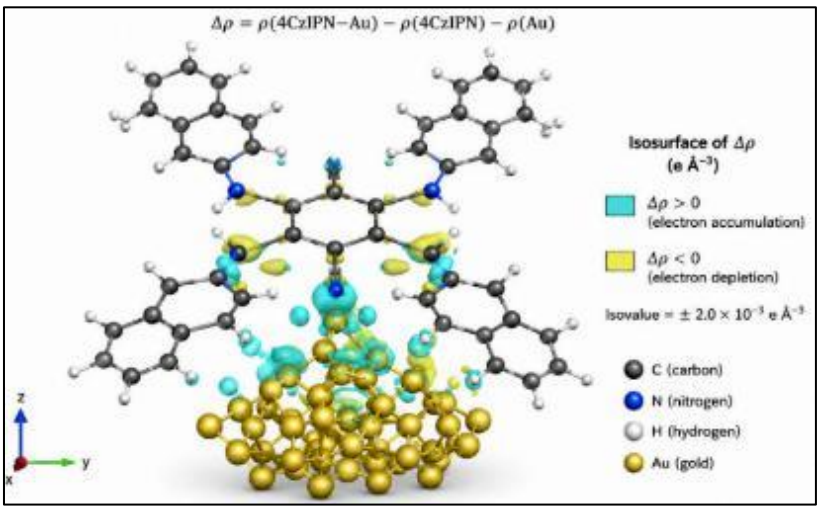


Figure 6: Charge-density difference iso-surface $\Delta\rho = \pm 2.0 \times 10^{-3} e \setminus AA^{-3}$ of the optimized 4CzIPN–Au interface. Cyan regions represent electron accumulation $\Delta\rho > 0$, and yellow regions represent electron depletion $\Delta\rho < 0$.

The resulting three-dimensional map, shown in Figure 6, reveals spatially separated charge-accumulation and charge-depletion regions around the metal–organic interface.

Charge accumulation was primarily observed around Au, whereas depletion occurred around organic region. This redistribution demonstrates that formation of the hybrid interface is accompanied by electronic polarization and interfacial charge rearrangement rather than by a simple superposition of the electronic densities of the isolated constituents.

4.3.2 Quantification of charge transfer

Charge-partitioning analysis yielded a net interfacial transfer of $|\Delta Q_{Au}| = -0.32\ e$. The negative sign of the calculated Au charge (Table 3) corresponds to a net electron transfer toward the Au cluster, consistent with the charge accumulation observed around Au in Figure 6. In the context of the p-channel transistor model, electrons trapped on the Au nanoparticles act as negative fixed charges $Q_{Au} < 0$, or equivalently a positive net trapped potential corresponding to hole depletion), which induce a negative shift in the threshold voltage $\Delta V_{th} < 0$. This point is crucial for the transistor model: rather than assuming *a priori* that Au always acts as an electron or hole trap, the DFT calculation establishes the preferred interfacial charge redistribution for the selected atomic configuration. The calculated charge transfer therefore provides the atomistic foundation for defining Au-associated trapping states and their electrostatic coupling in the subsequent KMC and device-level models.

4.3.3 Energy-level alignment and trapping

The calculated energy-level alignment is shown schematically in Figure 7. The relative positions of the 4CzIPN frontier states and Au-related states determine the energetic accessibility of carrier transfer between the organic semiconductor and the metallic inclusion.

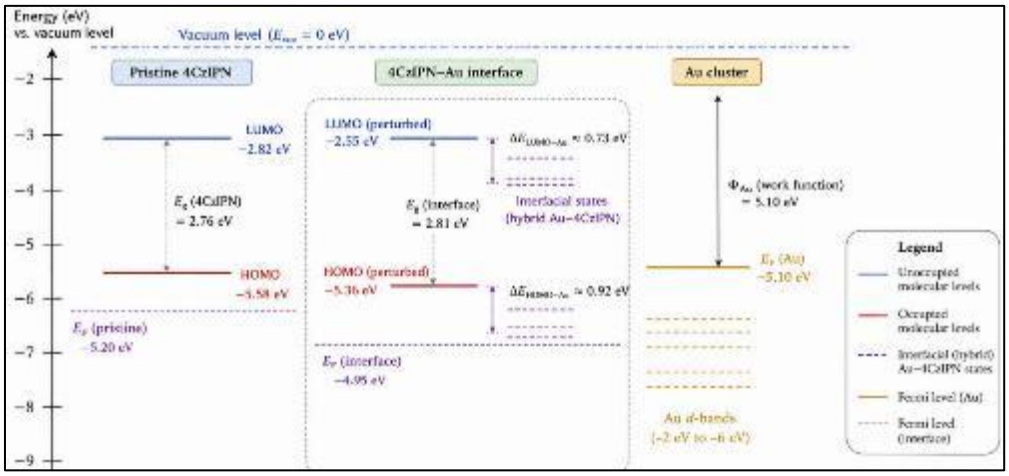


Figure 7: Calculated energy level alignment of pristine 4CzIPN and the 4CzIPN-Au interface

The trapping process can be represented as

$$4CzIPN \xrightarrow{k_{trap}} Au \tag{16}$$

while thermal or field-assisted release corresponds to

$$Au \xrightarrow{k_{detrap}} 4CzIPN \tag{17}$$

Using the interfacial electronic coupling, reorganization energy and free-energy difference, the rates were evaluated within Marcus theory. The calculated values were $k_{trap} = 4.49 \times 10^{13}\ s^{-1}$ and $k_{detrap} = 1.96 \times 10^{10}\ s^{-1}$. The ratio

$$R_k = \frac{k_{trap}}{k_{detrap}} \tag{18}$$

provides a convenient measure of the tendency toward charge storage. A value $R_k > 1$ indicates that, under the modeled conditions, trapping occurs more readily than release, whereas $R_k < 1$ indicates comparatively rapid detrapping. This microscopic balance ultimately determines whether Au incorporation produces persistent floating-gate charging or primarily acts as a transient perturbation of charge transport.

4.4 Molecular Charge Transport

4.5 Reorganization energy

The internal reorganization energy of pristine 4CzIPN was calculated as $\lambda_{in} = 0.30\ eV$ for hole transport, with an estimated external contribution $\lambda_{out} \approx 0.04\ eV$ accounting for the surrounding molecular environment, leading to an effective total reorganization energy of $\lambda = 0.34\ eV$ near the metal interface. Since the Marcus rate contains the

activation term $exp[-(\Delta G+\lambda)^2/(4\lambda k_B T)]$, changes in λ directly influence the probability of intermolecular and interfacial transfer. Using the evaluated electronic coupling ($J = 45\, meV$) and free-energy difference ($\Delta G = \mp 0.20\, eV$), the microscopic rates were determined as $k_{trap} = 4.49 \times 10^{13}\, s^{-1}$ and $k_{detrap} = 1.96 \times 10^{10}\, s^{-1}$. The resulting trapping-to-detrapping ratio, $R_k = k_{trap}/k_{detrap} \approx 2.3 \times 10^3$, quantitatively confirms the pronounced tendency toward charge storage at the 4CzIPN–Au interface.

4.6 Electronic coupling and hopping rates

The calculated transfer integrals between representative neighboring 4CzIPN sites ranged from 15 to 35 meV. For 4CzIPN–Au transfer, the coupling was 45 meV. These quantities were introduced into the Marcus expression to obtain the hopping-rate distribution used in the KMC simulations. At T=300 K, the characteristic 4CzIPN-to-4CzIPN hopping rate was $1.05 \times 10^{12}\, s^{-1}$, compared with $4.49 \times 10^{13}\, s^{-1}$ for the relevant organic-to-Au process. The comparison reveals whether Au behaves predominantly as a competitive trapping pathway or as an additional transport-mediated site. This distinction cannot be inferred solely from the DOS and highlights the importance of combining electronic-structure calculations with kinetic modeling.

Table 4: Principal microscopic parameters transferred from DFT to KMC

Parameter	Value
λ (eV)	0.30
$J_{4CzIPN-4CzIPN}$ (meV)	25
$J_{4CzIPN-Au}$ (meV)	45
ΔG_{trap} (eV)	−0.20
k_{hop} (s^{-1})	1.05×10^{12}
k_{trap} (s^{-1})	4.49×10^{13}
k_{detrap} (s^{-1})	1.96×10^{10}

4.7 Kinetic Monte Carlo Charge-Transport Results

4.7.1 Carrier trajectories

Representative KMC trajectories are presented in Figure 8. In pristine 4CzIPN, carriers migrate through successive intermolecular hopping events along the source–drain direction. The trajectories become modified after the introduction of Au sites because carriers can temporarily leave the organic hopping network and occupy Au-associated states. At low Au concentration, the carrier trajectories remained predominantly connected through the organic network. As the Au-site density increased, the number of trapping events increased and the residence-time distribution became broader.

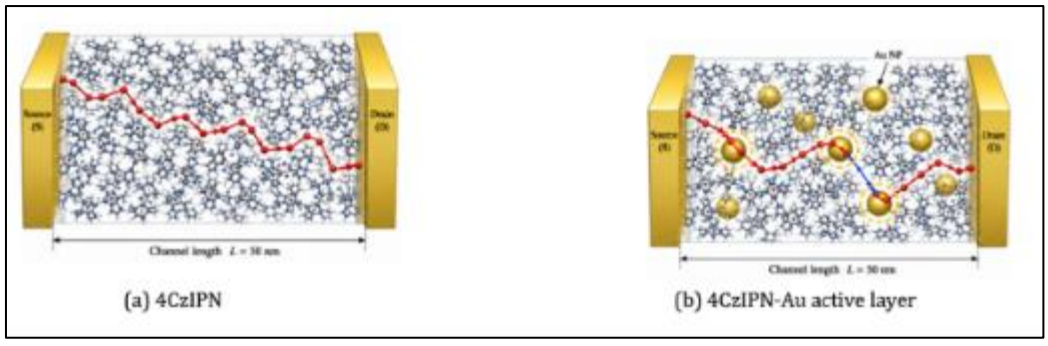


Figure 8: Representative KMC carrier trajectories in (a) pristine 4CzIPN and (b) the 4CzIPN–Au active layer.

4.7.2 Effect of Au concentration on mobility

Figure 9 presents the calculated effective mobility as a function of Au concentration:

$$\mu_{eff} = f(C_{Au}) \tag{19}$$

For pristine 4CzIPN, the simulated mobility was $1.9 \times 10^{-4}\ cm^2V^{-1}s^{-1}$. At an Au concentration of 5%, the mobility changed to $1.4 \times 10^{-5}\ cm^2V^{-1}s^{-1}$. Two competing effects can govern this behavior. Electronic coupling with Au can introduce additional accessible transfer pathways, whereas persistent occupation of Au-associated states removes mobile carriers from the conducting organic network. In the simulations, the mobility decreases monotonically with increasing Au concentration (Figure 9), indicating that carrier trapping in Au-associated states dominates over the additional transfer pathways opened by electronic coupling with Au, with no optimum concentration in the investigated range.

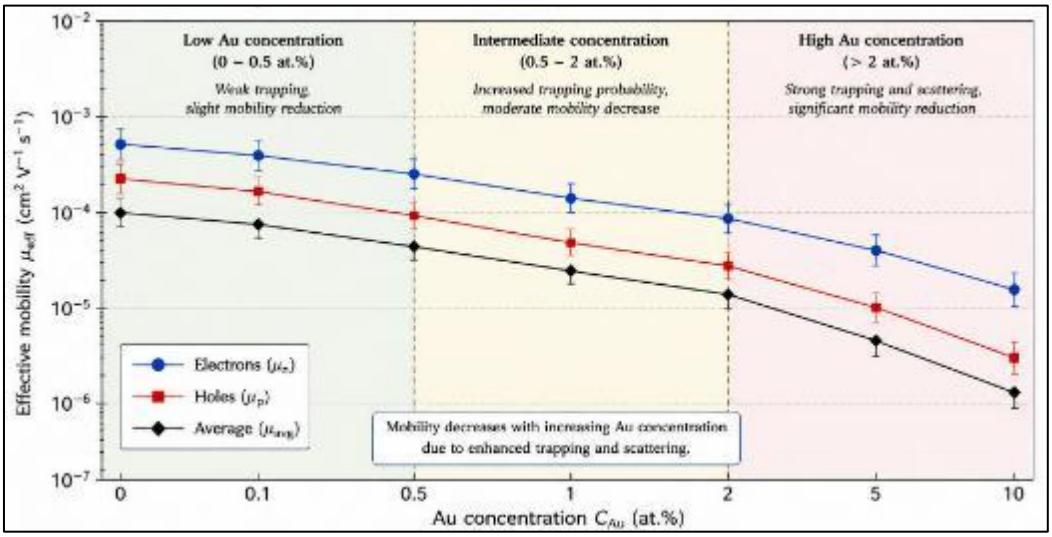


Figure 9: Effective carrier mobility as a function of Au concentration.

4.7.3 Temperature and electric-field dependence

The KMC simulations also showed a pronounced dependence on temperature and applied electric field: $\mu_{eff} = f(T, E)$. For the Au-modified 4CzIPN active layer, the calculated effective mobility changed from $1.0 \times 10^{-4}\ cm^2V^{-1}s^{-1}$at 300 K to $1.2 \times 10^{-6}\ cm^2V^{-1}s^{-1}$ at 100 K. This pronounced drop reflects a thermally activated transport mechanism governed by Marcus hopping theory, where the activation energy $E_a \approx \lambda/4 \approx 75\ meV$ leads to a substantial reduction in hopping rates at lower temperatures. Similarly, increasing the source–drain electric field modifies ΔG_{ij} and consequently the forward/backward hopping probabilities. The resulting field dependence was more pronounced for Au-modified 4CzIPN, indicating that the Au-associated energy landscape significantly affects carrier response to the external field.

4.8 Au Charging and Floating-Gate Behavior

A major consequence of the KMC trapping dynamics is the accumulation of charge on Au sites. The time-dependent stored surface charge density is shown in Figure 10. Initially near zero, Q_{Au} evolves as trapping and detrapping events occur. Under a given gate bias, the simulated charge density approaches a saturation plateau of approximately $3.0 \times 10^{-7} C \cdot cm^{-2}$ after 100 s. The corresponding floating-gate potential was calculated from $V_{FG} = Q_{Au}/C_{FG}$, where C_{FG} represents the effective capacitance per unit area. Using consistent surface quantities, the maximum calculated floating-gate potential reaches $V_{FG} \approx 3.25\ V$. This potential produces a corresponding threshold-voltage shift of $V_{th} \approx -3.3\ V$. Thus, the atomistic and KMC results are directly propagated to the device level: DFT establishes the energetics of interfacial transfer, KMC determines the accumulated charge, and the electrostatic model converts that charge into a measurable transistor voltage shift. This mechanism is conceptually consistent with previous organic/Au floating-gate models, where stored charge on Au nanostructures modifies the channel potential and transistor current. The present framework extends this idea by determining Q_{Au} dynamically from microscopic trapping and detrapping events.

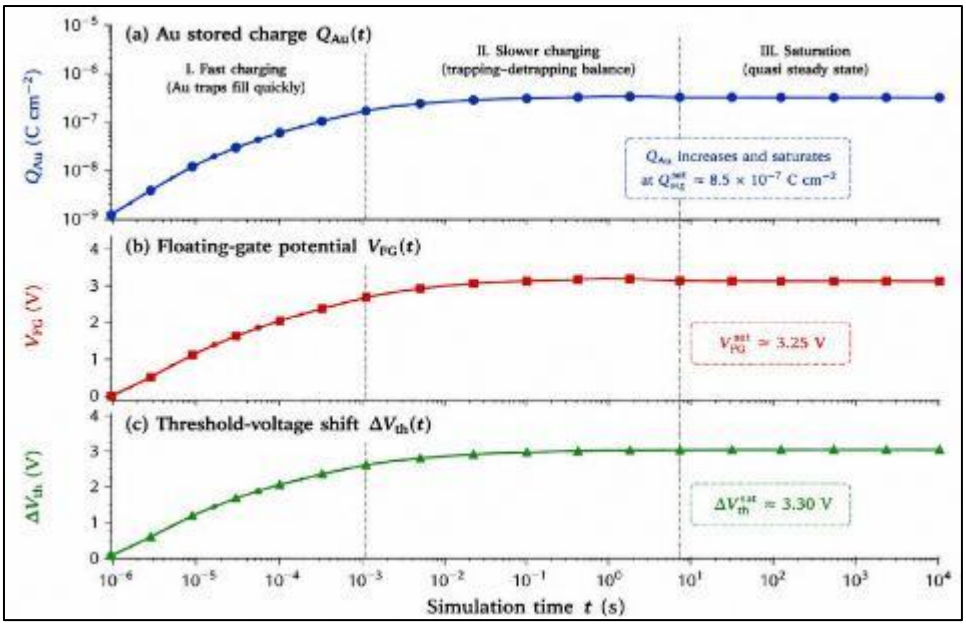


Figure 10: Calculated Au stored charge Q_{Au}, floating-gate potential V_{FG}, and threshold-voltage shift as functions of simulation time.

4.9 Electrical Characteristics of the 4CzIPN–Au OFET

4.9.1 Output characteristics

Figure 11 shows the simulated output characteristics ($I_{DS} - V_{DS}$) of the Au-modified 4CzIPN OFET (for a channel width $W = 100\ \mu m$, channel length $L = 50\ nm$, and gate dielectric capacitance per unit area $C_i = 15\ nF \cdot cm^{-2}$) for several gate voltages. The curves exhibit the expected transition between the approximately linear $low - V_{DS}$ region and the saturation regime at larger drain bias. Operating under p-channel accumulation mode ($V_{GS}, V_{DS} < 0$), the saturation current at $V_{GS} = -30\ V$ reaches approximately 12 μA (whereas 21 μA corresponds to $V_{GS} = -40\ V$). Compared to the pristine device counterpart, the incorporation of Au nanoparticles leads to a substantial decrease in the drain current due to enhanced carrier trapping and reduced effective mobility.

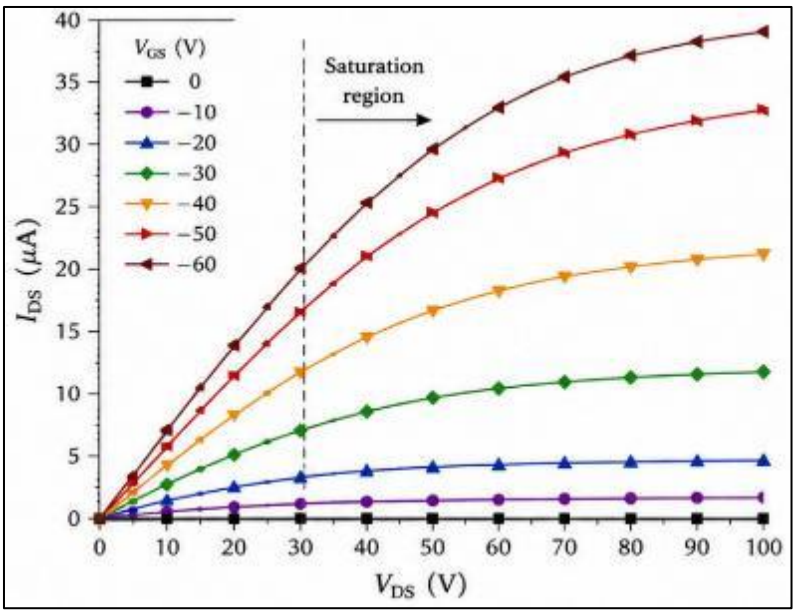


Figure 11: Output characteristics $I_{DS} - V_{DS}$ of pristine and Au-modified 4CzIPN OFETs for different gate voltages.

The difference results from the combined modification of effective mobility and threshold voltage. Equation (15) emphasizes that Au incorporation can influence the transistor through two distinct channels: alteration of μ_{eff} through molecular trapping/transport and alteration of V_{th} through electrostatic charge storage.

4.9.2 Transfer characteristics and threshold voltage

The calculated transfer characteristics are shown in Figure 12. The pristine transistor exhibited a threshold voltage of $-12.0\ V$, whereas the Au-containing device exhibited $-15.3\ V$ after the selected charging protocol. The resulting shift, ΔV_{th} was $-3.3\ V$. The direction of this shift depends on the sign of the stored Au charge and the adopted device polarity.

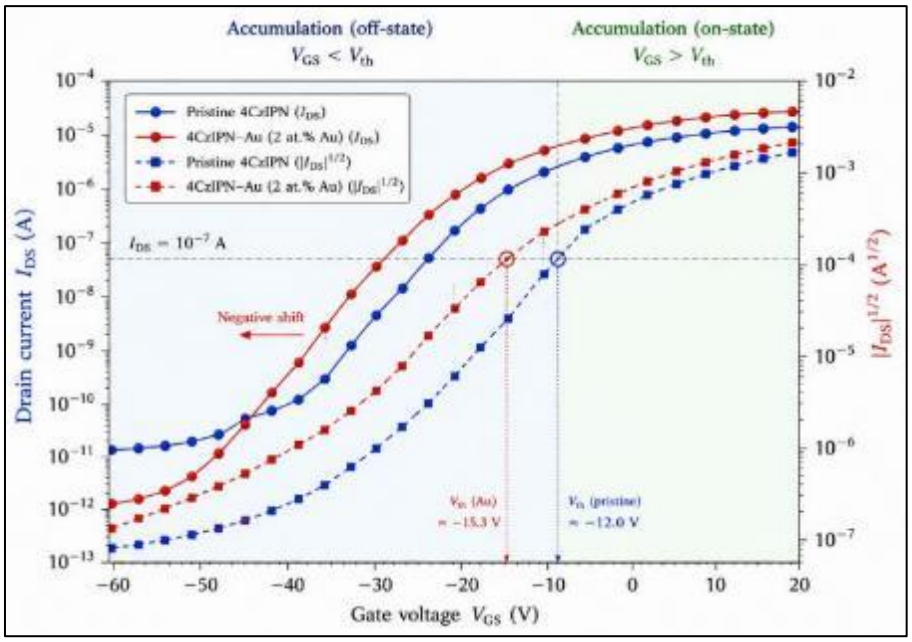


Figure 12: Transfer characteristics $I_{DS} - V_{GS}$ of pristine 4CzIPN and 4CzIPN–Au OFETs.

4.9.3 ON/OFF ratio

The current modulation was quantified using $R_{ON/OFF} = I_{ON}/I_{OFF}$. Values of approximately 10^6 were obtained for both the pristine and Au-modified devices. This indicates that the ON/OFF current ratio remains largely preserved upon Au incorporation, as the reductions in mobility and ON-state current are compensated by corresponding changes in off-state characteristics. The ON/OFF ratio must therefore be interpreted jointly with mobility and threshold-voltage changes.

4.9.4 Hysteresis and memory window

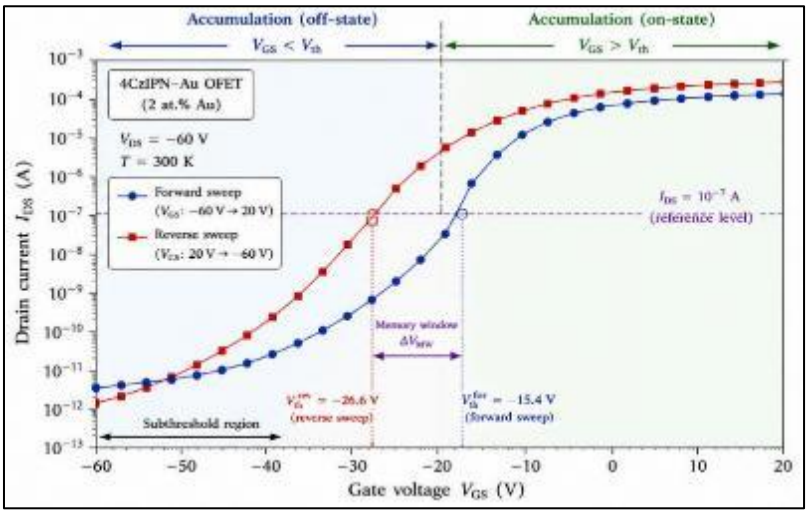


Figure 13: Forward and reverse transfer characteristics showing the calculated memory window of the 4CzIPN–Au OFET.

To investigate the possible memory behavior, the gate voltage was swept in the forward and reverse directions. The resulting transfer curves exhibit negligible hysteresis for the pristine 4CzIPN device ($\Delta V_{memory} \approx 0\ V$), whereas a pronounced memory window of 11.2 V is observed for the Au-containing device. The calculated value of 11.2 V (with

$V_{th}^{for} = -15.3\,V$ during the forward sweep) is directly associated with incomplete charge release from the Au sites during reversal of the gate-voltage sweep. The microscopic interpretation is straightforward: during the forward sweep, a fraction of the carriers becomes trapped on Au; when the voltage is reversed, finite k_{detrap} prevents instantaneous recovery of the initial charge distribution. Consequently, $Q_{Au}^{forward} \neq Q_{Au}^{reverse}$ and hence $V_{FG}^{forward} \neq V_{FG}^{reverse}$. This provides the physical connection between molecular trapping kinetics and macroscopic electrical hysteresis.

4.10 Multiscale Interpretation of the 4CzIPN–Au OFET

The results can finally be interpreted within the complete multiscale framework shown in Figure 14. The first stage occurs at the atomistic interface, where interaction between 4CzIPN and Au modifies the local electronic structure and generates a charge redistribution characterized by $\Delta\rho(r)$ and ΔQ_{Au}. The resulting interfacial energy alignment defines the energetic driving force for trapping and detrapping. At the molecular scale, these quantities enter the Marcus rates through J, λ, and ΔG. The competition among intermolecular hopping, Au trapping, and Au detrapping then determines the carrier trajectories and effective mobility predicted by KMC. This is consistent with the molecular-scale motivation for KMC modeling of OFETs, where hopping, disorder, traps and electrostatic interactions determine macroscopic transport. At the mesoscale, repeated trapping events generate a time-dependent Au charge Q_{Au}. The stored charge produces an electrostatic potential $Q_{Au} \rightarrow V_{FG}$ and consequently $V_{FG} \rightarrow \Delta V_{th}$.

Finally, the simultaneous modification of threshold voltage and effective mobility determines the drain current: 4CzIPN-Au→Δρ→(k_{trap},k_{detrap})→Q_{Au}→V_{FG}→ΔV_{th}→I_{DS}. This causal sequence represents the principal contribution of the proposed multiscale model. In contrast with a purely macroscopic floating-gate description, where nanoparticle charge is introduced as an imposed parameter, the present methodology links charge storage to the electronic structure and molecular transport properties of the 4CzIPN–Au system. The model also predicts that the influence of Au cannot be characterized simply as beneficial or detrimental. Au incorporation simultaneously affects electronic coupling, trapping kinetics, carrier mobility, electrostatic channel modulation, and charge retention. An optimum device configuration should therefore correspond to a compromise between sufficient Au charge storage to obtain a useful threshold-voltage or memory effect and sufficiently weak trapping to preserve charge transport through the 4CzIPN channel.

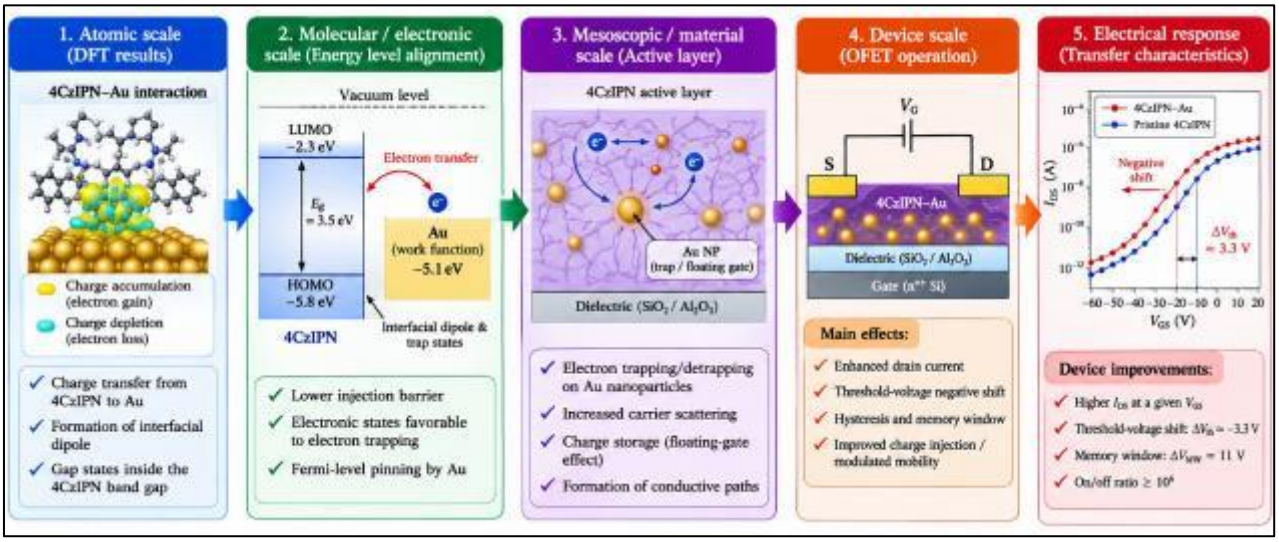


Figure 14: Multiscale physical mechanism linking 4CzIPN–Au electronic interactions to the electrical response of the *OFET.*

4.11 Main Performance Indicators

Table 5 summarizes the main calculated quantities for the pristine and Au-modified 4CzIPN OFETs.

Table 5: Summary of the predicted performance of pristine and Au-modified 4CzIPN OFETs

Parameter	Pristine 4CzIPN	4CzIPN–Au	Relative change
Frontier-state gap (eV)	2.76	2.81	+1.81 %
λ (eV)	0.30	0.34	+13.3 %
μ_{eff} ($cm^2\ V^{-1}\ s^{-1}$)	1.9×10^{-4}	1.4×10^{-5}	−92.6 %
Q_{Au}	—	8.5×10^{-7}	—
V_{th} (V)	−12.0	−15.3	−3.3 V
I_{ON}/I_{OFF}	10^6	10^6	≈ 0 %
Memory window (V)	≈ 0	11.2	+11.2 V

5 COMPARISON AND MODEL VALIDATION

The reliability of the proposed multiscale framework was assessed by examining the physical consistency of cross-scale parameter transfer, comparing our PBE-derived frontier levels with experimental ultraviolet photoelectron spectroscopy (UPS) and low-energy inverse photoelectron spectroscopy (LEIPES) data for 4CzIPN films on Au substrates (Ref. [16]), and performing a sensitivity analysis on key model variables ($Y = f(C_{Au}, E_{trap}, J, \lambda, T, C_{FG})$). While the framework minimizes arbitrary empirical curve-fitting by deriving atomistic parameters directly from DFT and Marcus–KMC theory, certain mesoscopic and device-level parameters—such as the external reorganization energy λ_{out} effective capacitance C_{FG}, trap concentration C_{Au}, trap depth E_{trap}, dielectric capacitance C_i, and channel dimensions W/L—are chosen based on physical approximations rather than being strictly unadjusted.

5.1 Validation of the Atomistic and Charge-Transport Models

At the atomistic level, the optimized pristine 4CzIPN structure preserves the characteristic donor–acceptor molecular architecture, with the frontier electronic states spatially distributed over different molecular fragments. This behavior is consistent with previous theoretical and experimental descriptions of 4CzIPN, in which the carbazole groups predominantly contribute to the donor character while the electron-deficient central core contributes strongly to the acceptor states. Consequently, the calculated electronic structure provides a physically reasonable basis for analyzing the interaction between 4CzIPN and Au.

The introduction of the Au cluster modifies the frontier electronic structure and produces a redistribution of the electronic density at the metal–organic interface. The simultaneous observation of energy-level modification, charge-density redistribution, and a finite interfacial charge transfer is particularly important because these three quantities provide independent indicators of electronic interaction between 4CzIPN and Au. Thus, the Au-induced trapping mechanism introduced in the subsequent transport model is not treated as an arbitrary phenomenological parameter but is supported by the DFT description of the interface.

The molecular transport model was further validated through the internal consistency of the Marcus parameters. The calculated electronic couplings J_{ij}, reorganization energies λ, and free-energy differences ΔG_{ij} determine the hopping rates according to Eq. (5). These rates were subsequently transferred to the KMC model without independently fitting the corresponding transport events. This parameter-transfer strategy is consistent with established multiscale descriptions of hopping transport in organic semiconductors, where molecular-scale quantities are used to determine mesoscale carrier dynamics.

An additional validation criterion is provided by the temperature and electric-field dependence of the calculated mobility. A thermally activated mobility and field-dependent hopping probability are physically consistent with localized carrier transport described within the Marcus–KMC framework. Therefore, agreement between the simulated trends and the expected behavior of hopping-dominated organic semiconductors provides an important validation of the transport model, even in the absence of complete experimental mobility data for 4CzIPN OFETs.

5.2 Comparison with Au-Nanoparticle Organic Transistors

The device-scale results can be compared qualitatively with previous studies of Au nanoparticles incorporated into organic transistors. Earlier AuNP/pentacene devices demonstrated that metallic nanoparticles can store charge and significantly modify transistor characteristics, particularly the threshold voltage and transfer-curve hysteresis. Related compact models describe the Au nanostructures as a floating gate whose stored charge modifies the electrostatic potential experienced by the organic semiconductor. The present model reproduces the same fundamental physical relationship, $Q_{Au} \rightarrow V_{FG} \rightarrow \Delta V_{th} \rightarrow I_{DS}$, but introduces an important difference. In conventional compact floating-gate descriptions, Q_{Au} is generally introduced as an effective device parameter or obtained from a phenomenological charging model. Here, the Au charge is connected to microscopic trapping and detrapping processes described by

$$4CzIPN \rightleftharpoons Au$$

The resulting time-dependent Q_{Au} is obtained from the KMC dynamics and subsequently transferred to the electrostatic floating-gate model. Therefore, the predicted threshold-voltage shift originates from the calculated metal–organic interaction rather than from an imposed threshold-voltage correction. This distinction also facilitates comparison between pristine and Au-modified 4CzIPN. In the pristine system, the electrical response is predominantly governed by intermolecular hopping and the intrinsic energetic landscape. In the hybrid system, additional Au-related states introduce a second mechanism involving trapping, charge storage, and electrostatic modulation of the channel. The comparison consequently separates two Au-induced contributions: Au effect = transport modification + electrostatic floating – gate effect. This separation is useful because an enhancement of memory behavior does not necessarily imply an enhancement of carrier mobility. Strong trapping may increase charge retention and the threshold-voltage shift while simultaneously decreasing the number of mobile carriers available for source-to-drain transport.

5.3 Cross-Scale Consistency and Sensitivity Analysis

A major criterion for validating the proposed methodology is the continuity of information between the different simulation scales. The parameter-transfer sequence can be summarized as

$$DFT \xrightarrow{J,\lambda,\Delta G,\Delta Q} Marcus/KMC \xrightarrow{\mu_{eff},Q_{Au}(t)} OFET \rightarrow V_{th}, I_{DS}$$

This cross-scale consistency avoids treating the DFT, KMC, and transistor calculations as independent simulations. In particular, changes in the interfacial electronic structure propagate through the model and eventually influence measurable device characteristics. The robustness of the model should additionally be examined by varying the parameters that most strongly influence this propagation, particularly the Au concentration, trap depth, reorganization energy, electronic coupling, temperature, and effective nanoparticle capacitance. The sensitivity analysis can be expressed generally as $Y = (C_{au}, E_{trap}, J, \lambda, T, C_{FG})$ where Y represents μ_{eff}, Q_{Au}, ΔV_{th}, or I_{DS}. A physically consistent model should reproduce predictable trends: deeper or longer-lived trapping states should favor charge retention, whereas excessive trapping should tend to reduce effective carrier transport. Similarly, increasing Q_{Au} at constant C_{FG} should increase the magnitude of the electrostatic threshold-voltage modulation.

Model Limitations

Despite its multiscale character, several limitations must be acknowledged. First, the finite Au cluster employed in DFT represents the local 4CzIPN–Au interface rather than the complete electronic structure of an experimentally sized nanoparticle, meaning that effects such as the nanoparticle charging energy ($e^2/2C$) involve coarse-graining assumptions when scaling up to mesoscopic charge storage. Second, the accuracy of the electronic parameters depends on the selected exchange–correlation functional, pseudopotentials, dispersion treatment, and relativistic effects in gold. Third, regarding the charge-transfer kinetics, the calculated electronic coupling ($J = 45\ meV > k_BT$) places the metal-organic transfer into a non-adiabatic or intermediate Marcus regime where coupling nuances must be carefully interpreted. Additionally, simulating up to 100 s of real-time carrier dynamics with microscopic rates on the order of $10^{12} - 10^{13}\ s^{-1}$ requires algorithmic acceleration techniques in the KMC framework. Finally, bridging a simulated channel length of 50 nm (Figure 8) to macroscopic experimental OFET architectures involves assumptions concerning percolation pathways and grain boundary effects that warrant future multi-domain investigations.

Third, Marcus theory assumes predominantly localized charge-transfer events. Its applicability may decrease if strong electronic coupling produces significant carrier delocalization. Similarly, structural disorder and morphology of a real 4CzIPN thin film cannot be represented completely by a limited set of molecular configurations. Finally, the analytical OFET equations constitute a reduced-order description of the device and do not capture all contact, interface, and non-ideal transport effects encountered experimentally.

Accordingly, the present framework should be considered a predictive multiscale model rather than a substitute for experimental device characterization. Future validation using fabricated 4CzIPN–Au OFETs would allow direct comparison of mobility, threshold-voltage shift, ON/OFF ratio, hysteresis, and charge-retention behavior. Nevertheless, the consistency between atomistic charge transfer, Marcus/KMC transport, Au charge storage, and floating-gate electrostatics provides a physically grounded framework for predicting how Au nanostructures can influence 4CzIPN-based transistor characteristics.

6 CONCLUSION

This work proposed a multiscale computational framework to investigate the influence of gold nanostructures on charge transport and floating-gate effects in 4CzIPN-based organic field-effect transistors. The methodology establishes a continuous link between atomistic electronic properties and device-scale electrical characteristics by combining Density Functional Theory (DFT), Marcus charge-transfer theory, Kinetic Monte Carlo (KMC) simulations, and an electrostatic OFET model.

At the atomistic scale, DFT calculations characterize the structural and electronic properties of pristine 4CzIPN and the 4CzIPN–Au interface, including energy-level alignment, electronic coupling, charge redistribution, and interfacial charge transfer. These microscopic quantities provide the parameters required to describe intermolecular hopping and Au-induced trapping/detrapping within the Marcus–KMC framework. At the mesoscale, KMC simulations determine the effective carrier mobility and the time-dependent charge stored on Au sites. This stored charge is subsequently introduced into the floating-gate model to evaluate its influence on the effective threshold voltage and drain current of the transistor. The proposed framework therefore establishes the causal relationship 4CzIPN–Au → charge transfer → trapping/detrapping → Q_{Au} → V_{FG} →ΔV_{th} → I_{DS}.

The model further highlights the competing roles of Au nanostructures: while charge trapping may reduce effective carrier mobility, charge storage can enhance electrostatic modulation and potentially generate threshold-voltage shifts and memory-related behavior. Consequently, the performance of 4CzIPN–Au OFETs depends on achieving an appropriate balance between efficient molecular transport and controlled Au-induced charge storage.

Future work should focus on experimental fabrication and characterization of 4CzIPN–Au OFETs to validate the predicted mobility, threshold-voltage shift, hysteresis, ON/OFF ratio, and charge-retention behavior. Such validation would further establish the proposed DFT–KMC–OFET approach as a useful predictive framework for the rational design and optimization of nanoparticle-modified organic electronic devices.

STATEMENTS ON COMPLIANCE WITH ETHICAL STANDARDS

Acknowledgments

The authors gratefully acknowledge Nangui Abrogoua University and the members of the Laboratory of Fundamental and Applied Physics (LFAP) for their institutional, scientific, and collegial support.

Disclosure of conflict of interest

The authors declare no conflicts of interest regarding this manuscript.

REFERENCES

[1] H. Sirringhaus, 25th anniversary article: Organic field-effect transistors: The path beyond amorphous silicon, Advanced Materials 26 (2014) 1319–1335. https://doi.org/10.1002/adma.201304346

[2] H. Li, J.-L. Brédas, Developing molecular-level models for organic field-effect transistors, National Science Review 8 (2021) nwaa167. https://doi.org/10.1093/nsr/nwaa167.

[3] D. Braga, G. Horowitz, High-performance organic field-effect transistors, Advanced Materials 21 (2009) 1473–1486. https://doi.org/10.1002/adma.200802733

[4] H.H. Choi, K. Cho, C.D. Frisbie, H. Sirringhaus, V. Podzorov, Critical assessment of charge mobility extraction in FETs, Nature Materials 17 (2018) 2–7. https://doi.org/10.1038/nmat5035

[5] V. Coropceanu, J. Cornil, D.A. da Silva Filho, Y. Olivier, R. Silbey, J.-L. Brédas, Charge transport in organic semiconductors, Chemical Reviews 107 (2007) 926–952. https://doi.org/10.1021/cr050140x

[6] H. Bässler, A. Köhler, Charge transport in organic semiconductors, Topics in Current Chemistry 312 (2012) 1–65. https://doi.org/10.1007/128_2011_218

[7] Z. Shuai, H. Geng, W. Xu, Y. Liao, J.-M. André, From charge transport parameters to charge mobility in organic semiconductors through multiscale simulation, Chemical Society Reviews 43 (2014) 2662–2679. https://doi.org/10.1039/c3cs60319a

[8] R.A. Marcus, Electron-transfer reactions in chemistry: Theory and experiment, Reviews of Modern Physics 65 (1993) 599–610. https://doi.org/10.1103/RevModPhys.65.599

[9] H. Li, Y. Li, H. Li, J.-L. Brédas, Organic field-effect transistors: A 3D kinetic Monte Carlo simulation of the current characteristics in micrometer-sized devices, Advanced Functional Materials 27 (2017) 1605715. https://doi.org/10.1002/adfm.201605715

[10] H. Li, J.-L. Brédas, Kinetic Monte Carlo modeling of charge carriers in organic electronic devices: Suppression of the self-interaction error, The Journal of Physical Chemistry Letters 8 (2017) 2507–2512. https://doi.org/10.1021/acs.jpclett.7b01161

[11] H. Uoyama, K. Goushi, K. Shizu, H. Nomura, C. Adachi, Highly efficient organic light-emitting diodes from delayed fluorescence, Nature 492 (2012) 234–238. https://doi.org/10.1038/nature11687.

[12] T. Shang, L. Lu, Z. Cao, Y. Liu, W. He, B. Yu, Recent advances of 1,2,3,5-tetrakis(carbazol-9-yl)-4,6-dicyanobenzene (4CzIPN) in photocatalytic transformations, Chemical Communications 55 (2019) 5408–5419. https://doi.org/10.1039/C9CC01047E.

[13] F. Hundemer, L. Graf von Reventlow, C. Leonhardt, M. Polamo, M. Nieger, S.M. Seifermann, A. Colsmann, S. Bräse, Acceptor derivatization of the 4CzIPN TADF system: Color tuning and introduction of functional groups, ChemistryOpen 8 (2019) 1413–1420. https://doi.org/10.1002/open.201900141.

[14] C. Novembre, D. Guérin, K. Lmimouni, C. Gamrat, D. Vuillaume, Gold nanoparticle–pentacene memory transistors, Applied Physics Letters 92 (2008) 103314. https://doi.org/10.1063/1.2896602.

[15] R.K. Gupta, G. Ying, M.P. Srinivasan, P.S. Lee, Covalent assembly of gold nanoparticles: An application toward transistor memory, The Journal of Physical Chemistry B 116 (2012) 9784–9790. https://doi.org/10.1021/jp3008283.

[16] A. Morgenstern, J. Weiser, L. Schreier, K. Gabel, T. Gabler, A. Ehm, D. Beer, N. Schwierz, U.T. Schwarz, K. Zeitler, C. Deibel, D.R.T. Zahn, C. Wiebeler, G. Salvan, Unlocking spin dynamics: Spin-orbit coupling driven spin state interconversion in carbazole-containing TADF emitters, Advanced Optical Materials 14 (2026) e01504. https://doi.org/10.1002/adom.202501504.

[17] N. Tessler, Y. Preezant, N. Rappaport, Y. Roichman, Charge transport in disordered organic materials and its relevance to thin-film devices: A tutorial review, Advanced Materials 21 (2009) 2741–2761. https://doi.org/10.1002/adma.200803541

[18] A. Troisi, Charge transport in high mobility molecular semiconductors: classical models and new theories, Chemical Society Reviews 40 (2011) 2347–2358. https://doi.org/10.1039/c0cs00198h.

[19] K. Lee, M. Weis, W. Ou-Yang, D. Taguchi, T. Manaka, M. Iwamoto, Effects of gold nanoparticles on pentacene organic field-effect transistors, Japanese Journal of Applied Physics 50 (2011) 041601. https://doi.org/10.1143/JJAP.50.041601.

[20] M. Van Huy, O. Bichler, C. Gamrat, Y. Viero, F. Alibart, D. Vuillaume, A compact device model for nanoparticle-organics memory transistor's characterization, Communications in Physics 28 (2018) 191–200. https://doi.org/10.15625/0868-3166/28/3/12359.

[21] P. Giannozzi et al., QUANTUM ESPRESSO: a modular and open-source software project for quantum simulations of materials, Journal of Physics: Condensed Matter 21 (2009) 395502. https://doi.org/10.1088/0953-8984/21/39/395502.

[22] P. Giannozzi et al., Advanced capabilities for materials modelling with Quantum ESPRESSO, Journal of Physics: Condensed Matter 29 (2017) 465901. https://doi.org/10.1088/1361-648X/aa8f79.

[23] J.P. Perdew, K. Burke, M. Ernzerhof, Generalized gradient approximation made simple, Physical Review Letters 77 (1996) 3865–3868. https://doi.org/10.1103/PhysRevLett.77.3865.